

# A Molecular Dynamics Study of a Reversed-Phase Liquid Chromatography Model

Joseph T. Slusher and Raymond D. Mountain\*

Physical and Chemical Properties Division, National Institute of Standards and Technology, 100 Bureau Drive, Stop 8380, Gaithersburg, Maryland 20899-8380

Received: October 8, 1998; In Final Form: December 28, 1998

We describe a molecular dynamics simulation study of a model of the reversed-phase chromatographic system. The model consists of a slab of aqueous solvent sandwiched between two walls having attached  $C_8$  hydrocarbon chains at a surface coverage of  $5.09 \mu\text{mol}/\text{m}^2$  or  $32.6 \text{ \AA}^2/\text{chain}$ . Long-ranged Coulombic interactions are taken into account using the Ewald sum method of Rhee et al. [*Phys. Rev. B* **1989**, *40*, 36]. The density and solvent orientation profiles are computed as a function of distance from the walls. The density profiles are found to be sensitive to the treatment of the long-ranged electrostatic interactions. The presence of an organic cosolvent (methanol or acetonitrile) at 30.8 mol % has little effect on the chain structure, which is largely collapsed against the walls. We also estimate the change in residual Helmholtz free energy along the pore width for a methane solute in the acetonitrile/water system, which indicates that a substantial portion of the free energy driving force for retention occurs in an organic-rich layer of solvent adsorbed to the hydrocarbon phase.

## 1. Introduction

The retention mechanism in reversed-phase liquid chromatography (RPLC) is an important problem in measurement technology that has received considerable attention in recent years.<sup>1,2</sup> A number of experimental methodologies have been brought to bear on the problem with varied and sometimes conflicting results.<sup>3</sup> The continuing interest in this area reflects the substantial difficulty in understanding the behavior (and thus our ability to predict/optimize) in these systems, which arises, in large part, from the inherent complexity in RPLC systems. One must address, in addition to state variables (i.e., temperature, pressure, flow rate), additional variables such as ligand density, chain length, and mobile phase composition, as well as the nature of the solute. Other important quantities, which are often unknown, are the surface coverage of exposed silanol groups<sup>4–6</sup> and the uniformity in surface density of the stationary alkyl chains.<sup>7</sup> A further difficulty in the analysis arises in the use of bulk thermodynamic treatments to describe a situation that is inherently interfacial.<sup>8</sup>

Some of the major questions that have been addressed have concerned the role of solvophobic vs chain–solute interactions,<sup>9</sup> the relative importance of partitioning vs adsorption,<sup>10</sup> the degree of solvent penetration into the stationary phase,<sup>11</sup> and the effect of the presence of microheterogeneities<sup>12,13</sup> or “layering” in mixed-solvent mobile phases.<sup>14</sup> Solute shape selectivities in relation to bonded-phase densities have also been addressed experimentally.<sup>11,15,16</sup>

A fruitful area of inquiry has dealt with the underlying bases for the different behavior seen in two commonly used RP mobile phases, aqueous methanol and aqueous acetonitrile. Here, thermodynamic measurements from van't Hoff plots of the mobile-phase composition dependence of the enthalpy ( $\Delta H^\circ$ ) and entropy ( $\Delta S^\circ$ ) of solute transfer (from mobile to stationary phases) show marked qualitatively different characteristics between the two systems. For instance, with aromatic solutes, several groups<sup>12,17,18</sup> have found that both  $\Delta H^\circ$  and  $\Delta S^\circ$  decrease

monotonically with increasing water volume fraction ( $\theta_w$ ) for the methanol/water system. In acetonitrile/water systems,  $\Delta H^\circ$  is independent of  $\theta_w$  while  $\Delta S^\circ$  increases with increasing  $\theta_w$  for  $\theta_w < 0.5$ . As a decrease in  $\Delta H^\circ$  indicates an increasing energetic preference while a decrease in  $\Delta S^\circ$  indicates a decreasing entropic preference for the stationary phase, these experiments suggest, for the acetonitrile system, an entropically governed retention process for  $\theta_w < 0.5$ . The molecular picture that emerges from the experimental results is one in which the solute is solvated by acetonitrile-rich pockets that exist in the water-poor mobile phase.<sup>12,19–21</sup> Hanai et al. have found similar trends in  $\Delta H^\circ$  and  $\Delta S^\circ$  for various other nonpolar solutes.<sup>22</sup> The microheterogeneous nature of acetonitrile/water mixtures at ambient temperatures has been indicated experimentally via Raman spectroscopy<sup>23</sup> as well as inverse Kirkwood–Buff studies<sup>24</sup> and is not surprising in view of the rather high upper critical solution temperature (272 K)<sup>19</sup> and the expectation of strong dipole–dipole interactions between acetonitrile molecules due to their linear shape and the relatively large dipole moment of acetonitrile (3.9 D).<sup>25</sup> In contrast to the acetonitrile/water system, enthalpic contributions to solute transfer are observed to dominate in the methanol/water systems.<sup>12</sup> Such comparative studies have contributed greatly to our overall understanding of the retention process in RPLC.

An important piece of information related to the retention mechanism in RPLC is the distribution of the solvent species in the vicinity of the stationary phase, where layering of both the alkyl chains and the mobile phase components is generally acknowledged. The preferential adsorption or intercalation of the organic component has been implicated in significant changes in the ordering of the stationary phase.<sup>13,26</sup> As it relates to  $\Delta S^\circ$ , such relative ordering effects in the stationary phase are likely to have a strong influence on the retention driving force.<sup>27,28</sup> In this regard, there are once again distinctly different mobile phases—stationary phase association characteristics between aqueous methanol and aqueous acetonitrile mobile phases.<sup>13,29</sup> Here, experimental evidence suggests that association between methanol and the stationary phase increases weakly

\* E-mail: RMountain@nist.gov. Fax: 301-869-4020.

with bulk methanol solvent composition, whereas that of acetonitrile saturates early and remains fairly constant. These authors also found differences in the association of water with the stationary phase between the two systems.

Molecular dynamics (MD) simulations offer the interesting possibility of addressing in a detailed way some of the molecular inferences suggested by the experimental measurements, under the assumption that the model system correctly captures the key features of the actual system. Recently, Klatte and Beck<sup>30</sup> used MD simulation to probe the driving forces that govern the retention process of a small nonpolar solute (methane) in a model system of 50/50 (v/v) water/methanol with a C<sub>18</sub> stationary phase. Their results, though not unambiguous, tend to support an interfacial rather than a bulk partitioning view of the retention process, where the bulk of the driving force is located at a methanol-rich layer at the interface. In the present work, we develop a similar MD model of the RPLC system in which we compare the solvation structure in a pure water system, a methanol/water system, and an acetonitrile/water system. The long-ranged goal of this work is to examine some of the features of these systems responsible for the retention mechanism, and to gain insight into the molecular picture of the microscopic differences in solvation structure among the three systems. Since there are a large number of variables to be considered such as chain length, chain density, solvent concentrations and composition, and solute species, among others, the results reported here should be viewed as a first step toward achieving the long-range goal. It should be noted that the current approach ignores the nonequilibrium nature of an actual chromatographic process by disregarding the flow field and its effects. This approach is necessary because the time-scale disparity between a typical flow velocity and the currently achievable length of a MD simulation is very large so that only simulations at equilibrium conditions are possible. However, insight into the equilibrium driving forces for retention and the mechanisms for solute selectivity is a foundational step toward a full understanding of solute retention in RPLC.

In the following section, the system model is described followed by a discussion of the technical details and the computation of the  $z$ -dependent chemical potential of an infinitely dilute solute. Finally, simulation results are presented for the  $z$ -dependence of the density, energy, pressure, solvent orientation and free energy, and some chain structure results.

## 2. Models and Simulation Methodology

**2.1. Models.** The system under study is a quasi-2-dimensional (2DP) one, with periodicity in the  $x$  and  $y$  directions but finite in the  $z$  direction. It is bounded by two “walls” representing the silica surface of the pore. The total potential energy of the system consists of *intermolecular* contributions from solvent–solvent, solute–solvent, solvent–chain, solute–chain, and chain–chain and *intramolecular* contributions in the chains. There are also interactions between all the molecules in the cell and both walls, and a springlike interaction that attaches the C<sub>8</sub> chains to the wall. With the exception of the latter, all of the intermolecular interactions are of the Lennard-Jones (LJ) form, with the addition of Coulombic terms for the solvent–solvent interactions.

In this work, we have taken a simple approach to the treatment of the wall interactions, although it would be possible to include explicit solvent–wall and chain–wall interactions. Explicit consideration of these interactions would make the model more realistic, e.g., by including solvent–silanol interactions, which may be an important part of the overall picture of solute

retention. In this initial work we have chosen the much more computationally efficient route of treating the walls as flat, featureless surfaces by using a 10-4-3 potential<sup>31</sup> that provides a better representation of the surface interaction than the 9-3 potential obtained by integrating a LJ potential. The wall potential is

$$U^{\text{wall}} = 2\pi\epsilon_w \left\{ 0.4 \left( \frac{\sigma_w}{z} \right)^{10} - \left( \frac{\sigma_w}{z} \right)^4 - \frac{C_1}{(z/\sigma_w + C_2)^3} \right\} \quad (1)$$

where  $C_1 = 0.471\,404\,52$  and  $C_2 = 0.431\,335\,136$  are constants, and  $\sigma_w$  and  $\sigma_w$  are taken as  $\sigma_{\text{OO}}$  and  $\sigma_{\text{OO}}$  of the water model. Although we are aware that the molecular details of the silica may be important, the neglect of the wall details is probably a reasonable approximation for the relatively high surface coverage studied here and particularly for the specific case of a nonpolar solute, which would not be expected to interact appreciably with any exposed silanol groups.

The C<sub>8</sub> chains are modeled in the united-atom approximation, including both bending and torsion (but not stretching), and an intramolecular LJ interaction between sites more than three bonds apart.<sup>32</sup> The bending potential is given by<sup>33</sup>

$$U^{\text{bend}}(\theta) = \frac{1}{2}c_\theta(\theta - \theta_o)^2 \quad (2)$$

where  $c_\theta/k_b$  is  $3.018\,846 \times 10^4$  K/rad<sup>2</sup> and  $\theta = 109.5^\circ$ . The torsional potential acts on five sets of four sites within a C<sub>8</sub> chain and is given by<sup>32</sup>

$$U^{\text{tors}}(\phi) = \sum_{k=0}^5 c_k (\cos \phi)^k \quad (3)$$

where  $\phi$  is the dihedral angle defined so that  $\phi = 0$  corresponds to the trans configuration, and the constants  $c_k$  are  $c_0/k_b = 1.116 \times 10^3$  K,  $c_1/k_b = 1.462 \times 10^3$  K,  $c_2/k_b = -1.578 \times 10^3$  K,  $c_3/k_b = -3.68 \times 10^2$  K,  $c_4/k_b = 3.156 \times 10^3$  K, and  $c_5/k_b = -3.788 \times 10^3$  K. The intramolecular forces arising from the torsional interaction acting on contiguous sites  $i, j, k$ , and  $l$  have been derived by following the development of Bekker et al.<sup>34</sup>

The chains are fixed to the wall with an arbitrary spring potential having a stiff constant, acting between a position approximately 3 Å from the wall and the first site of the chain,  $r_1$ ,

$$U^{\text{spring}} = c_{\text{spring}}(r_1 - r_o)^2 \quad (4)$$

with  $c_{\text{spring}}/k_b = 2.27 \times 10^4$  K/Å<sup>2</sup>. In an attempt to mimic the assumed roughness of the surface of the silica pore, the chains are initially allowed to move freely in the  $x$ ,  $y$ , and  $z$  directions for about 0.5–1 ps before fixing the locations of the end sites at  $r_o$ . The resulting positions of  $r_o$  were within  $3 \pm 1.5$  Å from the wall.

For the solvent water, we adopt the SPC potential,<sup>35</sup> for methanol the potential parameters of van Leeuwen,<sup>36</sup> and for acetonitrile the model of Edwards et al.<sup>37</sup> The parameters for the intermolecular potentials are collected in Tables 1 and 2. For unlike sites, the Lennard-Jones parameters are obtained via the usual Lorentz–Berthelot combining rules, i.e.,  $\sigma_{\alpha\beta} = (\sigma_\alpha + \sigma_\beta)/2$  and  $\epsilon_{\alpha\beta} = (\epsilon_\alpha\epsilon_\beta)^{1/2}$ .

The system contained a total of 500 solvent molecules and 50 C<sub>8</sub> chains. Half of the chains are attached to each wall. The equations of motion were solved with a time step of 1.019 fs

**TABLE 1: Geometrical Parameters for Molecular Models**

molecule	bond	length (nm)	bond angle	degrees
SPC water	O—H	0.1008	HOH	109.47
L1 methanol	C—O	0.14246	COH	108.53
	O—H	0.09451		
acetonitrile	CH <sub>3</sub> —C	0.146		
	C—N	0.117		
C <sub>8</sub>	C—C	0.153	CCC	109.5

**TABLE 2: Pair Potential Parameters**

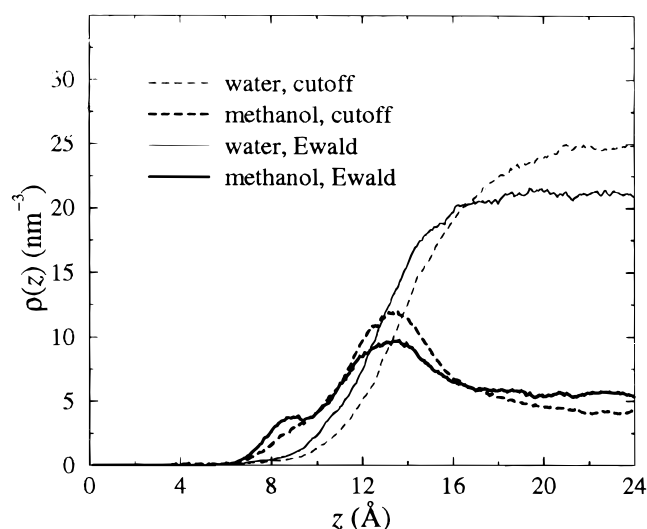
molecule	group	$\sigma$ (nm)	$\epsilon/k_b$ (K)	q
SPC water	O	0.3166	77.92	-0.820
	H	0	0	0.410
L1 methanol	O	0.303	86.5	-0.700
	CH <sub>3</sub>	0.3740	105.2	0.265
	H	0.00	0.000	0.435
acetonitrile	CH <sub>3</sub>	0.360	191.0	0.269
	C	0.340	50.0	0.129
	N	0.330	50.0	-0.398
C <sub>8</sub>	CH <sub>n</sub>	0.396	72.9558	0.000

using noniterative constraint dynamics<sup>38</sup> with the Beeman algorithm<sup>39</sup> and a Nosé—Hoover thermostat<sup>40</sup> to control the temperature.

**2.2. Technical Issues.** In Coulombic systems having broken symmetry in one direction, it has been shown that the use of the usual formulation of the Ewald sum for 3-dimensional periodicity (3DP) is inappropriate.<sup>41,42</sup> This is true because use of the 3DP formulation in a system having 2D periodicity in the  $x$  and  $y$  directions, but which is finite in the  $z$  direction, would introduce spurious effects of charge layers perpendicular to the  $z$  direction that are not part of the system. The imposition of a large “vacuum” region in the  $z$  direction has sometimes been used to simulate systems with broken translational symmetry,<sup>43,44</sup> but the consequences of this approximation are not understood. Thus, to rigorously deal with the long-ranged Coulombic interactions in such a system, an alternate Ewald-like method must be used.

A recent review of some of these approaches can be found in ref 45. Generally, a particular method is computationally feasible within only a rather narrow geometric arrangement of the charges. Outside of this range, the methods either contain singularities or experience convergence problems. For instance, the recent method of Hautman and Klein<sup>46</sup> converges slowly when  $z/L$  becomes large i.e., close to 1. ( $L = L_x = L_y$  is the length of the simulation box in the direction of periodicity.) This particular method also depends on inverse powers of the intermolecular distance in the  $x$ – $y$  plane,  $s$ , a feature that can also cause numerical difficulties when two charges are stacked in the  $z$  direction. An alternative approach derived by Leckner<sup>47</sup> was considered briefly but not implemented as the computational effort is large for near-neighbor molecules. A method that does not suffer from charge geometry convergence problems has been proposed by Heyes et al.<sup>48</sup> However, because of a complicated  $z$ -dependence in the Fourier part, this formulation is exceedingly slow. No particular method has emerged as clearly the best approach for the general simulation.

We have chosen to use the method proposed by Rhee et al.,<sup>41</sup> which combines an Ewald-like sum with a multipole expansion in the  $z$  direction. Although this method unfortunately suffers from one of the same problems as does the Hautman–Klein method, i.e., poor accuracy when the  $z$  separation becomes larger than  $L$ , it has an advantage over the latter in that it does not depend on inverse powers of  $s$ . Both the Rhee et al. and the Hautman–Klein methods enjoy a further numerical advantage by eliminating the  $z$ -dependence in the Fourier part of the sum,

**Figure 1.** Comparison of density profiles for the oxygen site of water and methanol with spherical truncation of Coulombic interactions and Ewald sum.

allowing it to be factored. Relative to the 3DP Ewald sum, however, the computational requirements of any of the 2DP formulations are much more severe. With the present implementation of the Rhee et al. method used in this work, the necessity of including an extra layer of simulation cell images in the real-space portion of the sum decreases the speed by 1 order of magnitude relative to the 3DP Ewald sum.

The use of an Ewald sum to rigorously deal with the long-ranged Coulombic interactions is very expensive computationally. However, spherical truncation of these interactions can have a significant effect on the computed results. This is illustrated in Figure 1, in which the density profiles are compared in the methanol/water system for the Ewald sum and for spherical cutoff (based on solvent–solvent center-of-mass distances). For the latter case, the sharpness of the interface is underestimated while the layering of the methanol is overestimated.

For the sake of completeness, we include in the Appendix the expressions for the Coulombic energy and force for the multisite molecular case and derive expressions for the pressure tensor in both the “atomic” and “molecular” frameworks.

**2.3. Numerical Accuracy of Coulombic Interactions.** Although the use of the above Ewald sum is computationally expensive, neglect of the long-ranged forces can have a large effect on the accuracy of the Coulombic contribution to the forces. In Figure 2, we compare the accuracy in the forces for two different schemes: spherical cutoff based on center of mass to center of mass minimum image (MI) distances being less than 0.86 nm and the Rhee et al. Ewald formulation with a real-space MI site–site cutoff at  $\nu_c = 1$ , (i.e., nine cells in the real-space sum) and a convergence parameter  $\alpha/L = 0.1$ . The forces are normalized to the essentially exact results found when  $\nu_c = 2$ . The results are shown for a snapshot configuration from the pure water system, where the effective ratio of  $L_z$  to  $L$  is about 0.92 due to the exclusion of water from near the walls by the hydrocarbon chains. In both cases, the contribution to the forces from the multipole expansion is included. The average absolute errors in the forces with the Ewald sum ( $\nu_c = 1$ ) are 0.72%, 0.73%, and 0.65% for the  $x$ ,  $y$ , and  $z$  directions. The corresponding errors for spherical cutoff are very large: 33%, 31%, and 20%.

To make the computations feasible, the simulation code was parallelized with the “data-replication” approach. The message passing interface (MPI) library was used in the global summa-



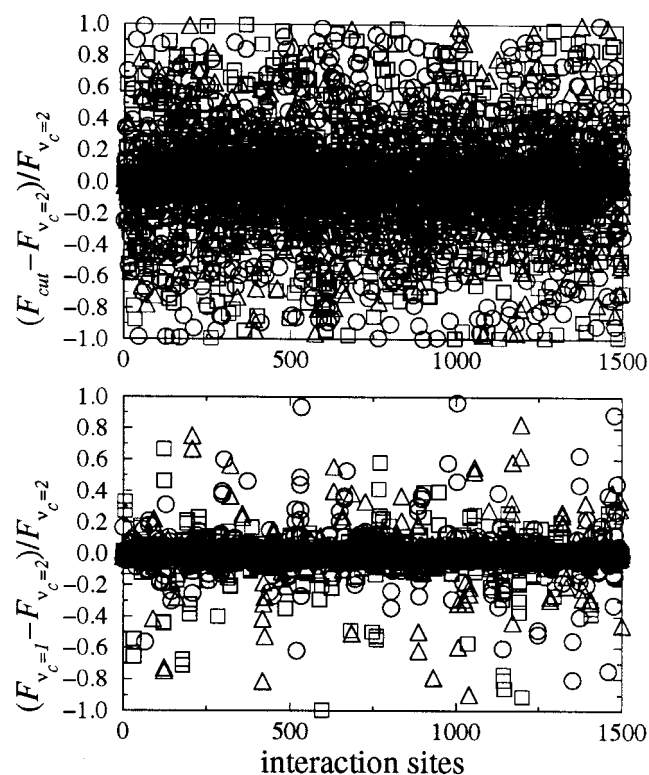


**Figure 2.** Error in Coulombic contribution to site-site forces in the  $x$  ( $\circ$ ),  $y$  ( $\square$ ), and  $z$  ( $\triangle$ ) directions for a typical configuration in the water/ $C_8$  system. The 1500 interaction sites are the locations of the oxygen and hydrogen sites on the 500 water molecules in the system and are not in any particular order.

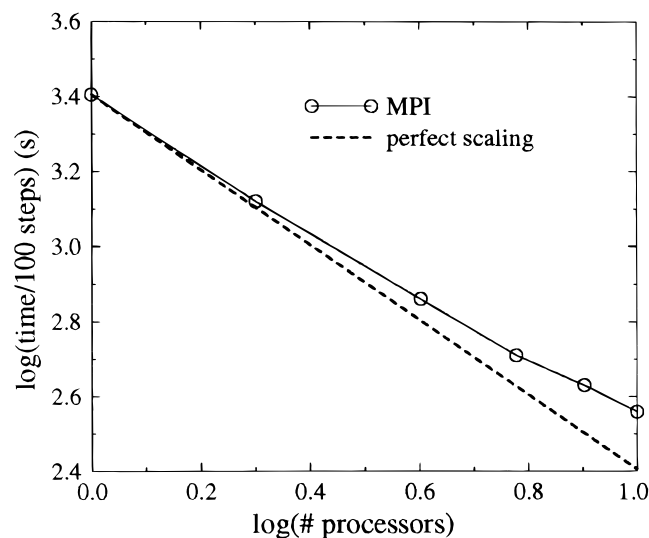


**Figure 3.** Wall-clock time needed to integrate through 100 time steps using different numbers of processors, for the system of 500 water molecules with 50  $C_8$  chains.

tion of the forces, energies, etc. in order to allow portability to various architectures. From the timings for various numbers of processors on an IBM SP2, shown in Figure 3, it can be seen that nearly linear speed-up is obtained for up to 10 processors. Above this number, message-passing overhead begins to dominate the timings.

### 3. Free Energy Profile

The change in free energy of a solute as it experiences different microenvironments in a RPLC column is the basic

driving force in the retention process. In this way, the solute acts as a probe to determine whether the retention is primarily driven by solute-solvent interactions or interactions between the solute and the stationary phase and whether the process is primarily an interfacial one or if it resembles a bulk partitioning process. The simulation results of Klatt<sup>30</sup> and Beck<sup>30</sup> suggest, at least for small, spherical, nonpolar solutes, that the process is largely interfacial. For nonspherical solutes, free energy profiles obtained from MD simulations can be used to test ideas such as the slot model<sup>49</sup> and the effects of stationary-phase surface coverage on the partitioning. The information we seek is the change in free energy, in this case the residual Helmholtz free energy, of a solute  $A^{\text{res}}$  at infinite dilution in the model RPLC system, as a function of distance along the  $z$  coordinate.

The  $z$ -dependence of the Helmholtz free energy could be calculated from the  $z$ -dependence of the partition function,

$$A^{\text{res}}(z) = -k_b T Q(z) \quad (5)$$

and then relating the  $z$ -dependence of the partition function to the probability of finding the solute at a specific  $z$  position within the simulation cell. However, such an approach would suffer from extremely poor statistics since the range of possible  $z$  values is large and we have only one solute molecule. To overcome this problem, we adopt a commonly used umbrella sampling scheme<sup>30,50</sup> where the position of the solute is constrained to lie within a certain window of  $z$  values. In this case, the configurational energy of the solute is due to solute-solvent, solute-chain, and solute-wall interactions, plus the well potential. The  $z$  position of the solute is constrained to lie within a narrow range of  $z$  by applying a well potential to the center of mass or a site near the center of the molecule,

$$U^{\text{well}}(z; z_0) = \epsilon_z \left( \frac{z - z_0}{\sigma_z} \right)^{12} \quad (6)$$

with arbitrarily chosen values  $\sigma_z = 0.7675 \text{ \AA}$  and  $\epsilon_z/k_b = 8.553 \times 10^4 \text{ K}$ . The solute is then allowed translational freedom in the  $x$  and  $y$  directions as well as rotational freedom. Within the window, the  $z$ -dependent free energy of the system in the absence of the well potential is

$$A^{\text{res}}(z) = -k_b T \ln P(z) - U^{\text{well}}(z; z_0) \quad (7)$$

where  $P(z)$  is the probability of finding the solute at a position  $z$  within the window in the presence of the well potential. In practice,  $P(z)$  is calculated for a number of contiguous windows and then normalized. The free energy profile is then constructed by requiring the free energy to be the same at the overlap between two windows.

### 4. Results and Discussion

Table 3 lists the relevant details of the simulations, and some of the computed thermodynamic properties at the center of the slit pore are given in Table 4. No attempt has been made to include long-ranged corrections to the LJ contributions for any of the computed properties.

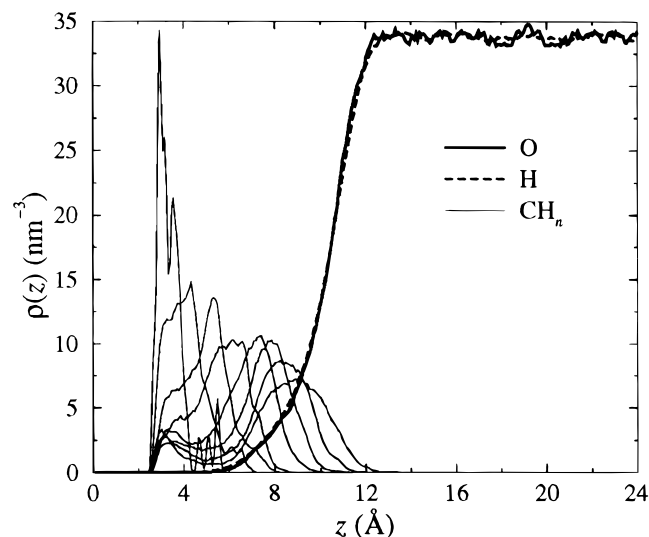
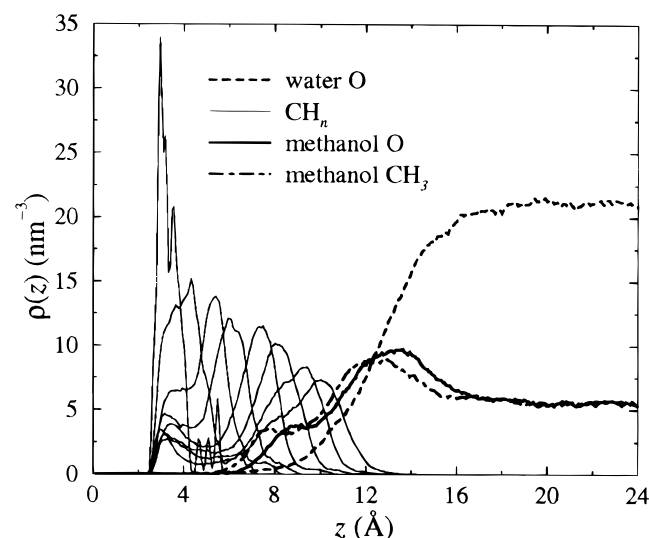
**4.1. Density Profiles.** The site density profiles have been computed using a bin width of  $0.07675 \text{ \AA}$  and are shown in Figures 4–6 for the three different systems. In the pure water system, the interface between the water and alkyl chain phases is fairly sharp, although there is some degree of penetration of

**TABLE 3: State Point and Configurational Energy**

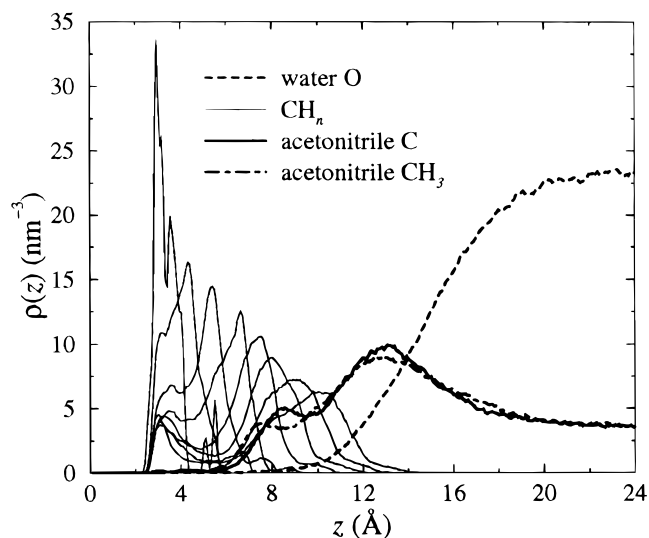
system	$N_o$	$N_w$	$N_{\text{chain}}$	$L$ (nm)	$L_z$ (nm)	$T$ (K)	$P$ (MPa) <sup>a</sup>	$U^c$ (kJ/mol) <sup>a</sup>	$\tau^b$ (ps)
ACN	154	346	50	2.855	4.789	305.9	83(3)	-36.1(1)	403
MeOH	154	346	50	2.855	4.544	298.0	-2(3)	-36.6(1)	371
Water	0	500	50	2.855	3.838	298.0	18(5)	-37.5(1)	258

<sup>a</sup> Standard uncertainty in last digit given in parentheses. <sup>b</sup> Simulation length.**TABLE 4: Conditions at Center of Pore**

system	$\rho_o$ (g/cm <sup>3</sup> )	$\rho_w$ (g/cm <sup>3</sup> )	$P$ (MPa)	$x_o^a$
ACN	0.252	0.692	80	0.138
MeOH	0.297	0.633	24	0.209
Water		1.011	61	

**Figure 4.** Number densities as a function of  $z$  for the pure water system.**Figure 5.** Number densities as a function of  $z$  for the methanol/water system.

the water ( $w$ ) into the nonpolar phase by about 5 Å. Unlike the case of a hard or rigid wall,<sup>51–54</sup> where large density fluctuations are seen in the water density near the interface, the present results show a relatively flat profile with the water quickly reaching its bulk density ( $\approx 1.0$  g/cm<sup>3</sup>). This behavior is similar to that seen at the interface between water and a bulk hydrocarbon liquid<sup>55</sup> and is likely due to a “smearing-out” effect

**Figure 6.** Number densities as a function of  $z$  for the acetonitrile/water system.

of the water density profile due to undulatory fluctuations in the surface of the hydrocarbon phase.<sup>56,57</sup> A slight separation in the H and O profiles can also be seen, which indicates the existence of a slight degree of orientational ordering of the water molecules near the interface.

In the mixed solvent systems (Figures 5 and 6), there is a striking segregation of the organic ( $o$ ) component at the interface. This buildup of the organic component excludes water from the interface, as shown by the location of the Gibbs dividing surface of the water,  $z_G$ , defined by the condition

$$\int_0^{z_G} \rho_w(z) dz = - \int_{z_G}^{z_C} (\rho_w(z) - \rho_{w,C}) dz \quad (8)$$

where  $\rho_w$  is the number density of water and  $\rho_{w,C}$  is the density of the water at the center of the pore,  $z_C$ . The values of  $z_G$  are 10.2, 12.6, and 14.7 Å for the pure water, methanol/water, and acetonitrile/water systems, respectively. In the water/methanol system, the alcohol concentration in a layer approximately 5 Å in thickness near the chain surfaces is nearly twice its value in the bulk. One can also clearly see a preferential orientation of the methanol in this region, as has been previously noted,<sup>30</sup> with the methyl group pointing toward the hydrocarbon phase while the hydroxyl group maximizes its H-bonding interactions with the water. The layering of the organic phase near the interfaces is qualitatively similar in the acetonitrile/water system, where it is even more pronounced. Here the peak interfacial concentration of acetonitrile exceeds twice the value near the center of the pore and the thickness of the layer is 6–7 Å. Both the acetonitrile and the methanol penetrate into the hydrocarbon phase to approximately the same degree, with primary and secondary peaks in the densities occurring at the surface and several angstroms into the surface. Unlike the methanol/water system, where the presence of the methanol tends to pull some

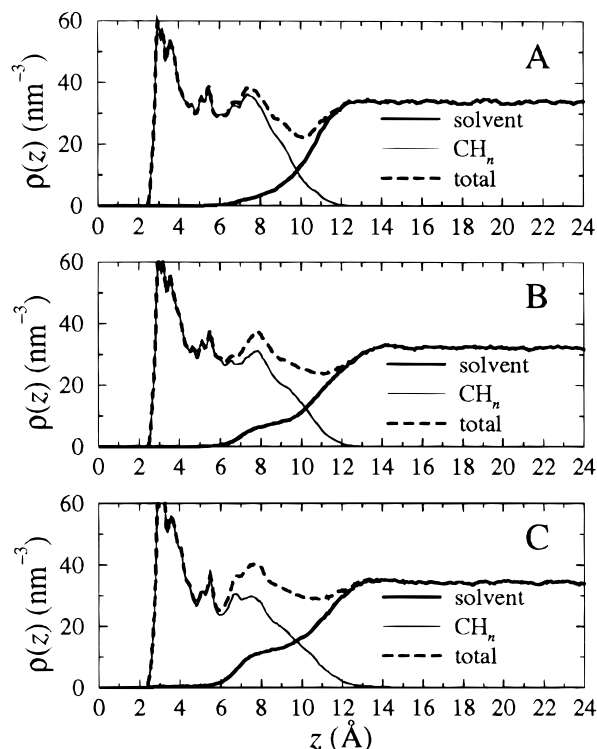


**Figure 7.** Total density of LJ interaction sites as a function of  $z$  for the (A) pure water system, (B) methanol/water system, and (C) acetonitrile/water system.

of the water into the hydrocarbon phase, in the acetonitrile/water system interfacial acetonitrile tends to exclude water from the interface because of the much weaker acetonitrile–water interactions. Additionally, the density profiles for acetonitrile do not indicate a significant amount of orientational ordering of the acetonitrile molecules at the interface.

The total site number densities along the  $z$  coordinate (Figure 7) reveal a sharp interface in the pure water system that becomes less sharp in the water/methanol system and is quite diffuse in the acetonitrile/water system. These data also indicate the presence of small density peaks due to alkyl chain layering.

**4.2. Chain Structure.** An important question related to the retention mechanism in RPLC is the effect of different mobile phases on the ordering of the stationary phase. The expectation has been that disordered or folded states predominate with poor chain solvents such as water, while solvation of the chains with an organic component favors chain extension and ordering.<sup>26,58,59</sup> Three quantities that give a measure of the chain structure from the simulations are the distribution of the angle  $\chi$ , defined as

$$\cos \chi \equiv \hat{\mathbf{r}}_{18} \cdot \hat{\mathbf{z}} \quad (9)$$

where  $\mathbf{r}_{18} = \mathbf{r}_8 - \mathbf{r}_1$  and  $\hat{\mathbf{z}}$  is a unit normal to the wall, the distribution of the end–end distance of the alkyl chains,  $r_{\text{end-end}}$ , and the center of mass of the hydrocarbon layer,

$$\langle z \rangle \equiv \int_0^{z_c} z \rho_s(z) dz / \int_0^{z_c} \rho_s(z) dz \quad (10)$$

where  $\rho_s(z)$  is the total number density of the  $\text{CH}_n$  sites of the chains. The distributions of  $\chi$  and  $r_{\text{end-end}}$  are compared in Figure 8 for the three systems. We note first that the values of  $\chi$  are bimodally distributed with a tendency for the chains to either extend away from the surface or to lie nearly flat in an

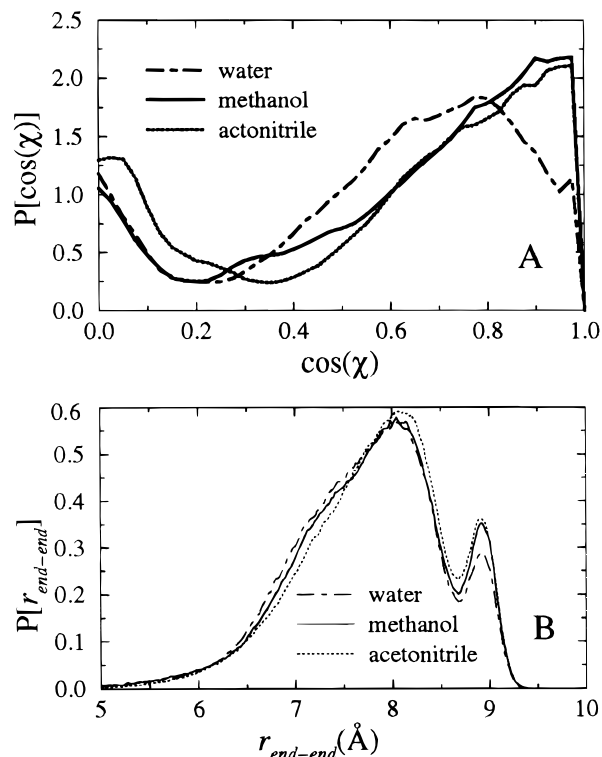


**Figure 8.** Probability density of chain–wall normal angle (A) and chain end–end distance (B) for different systems.

orientation parallel to the walls. Apparently, the interaction of the chains with the wall potential begins to predominate when the chains begin to lie close to the wall. Given the rather limited flexibility in  $\text{C}_8$  chains, there is little difference in the results for the different systems, particularly since the hydrophobic nature of the solvent has not changed greatly among the three systems. The statistically indistinguishable values of  $\langle z \rangle$  support this observation, being 5.92, 5.97, and 6.00 Å for the water, acetonitrile/water, and methanol/water systems, respectively. From the distributions of  $\chi$ , we can tentatively conclude that the occurrence of nearly straight chains perpendicular to the walls is slightly diminished in the pure water systems relative to the others. Such distinctions are likely to be much more pronounced in systems having longer alkyl chains, such as  $\text{C}_{18}$ . We are currently performing a detailed analysis of the effect of solvent composition on the  $\text{C}_{18}$  conformational order. Interestingly, Sander et al.,<sup>26</sup> using infrared spectrometry, found marked differences in the  $\text{C}_{18}$  alkyl chain conformation for dry RPLC packings compared to those in the presence of a mobile phase. However, they did not detect any significant changes in the IR spectra with mobile phase compositions in organic-rich (70% to 100%) methanol/water solutions.

The  $r_{\text{end-end}}$  distribution is also bimodal with a peak at about 8.9 Å corresponding to the nearly all-trans configuration. The broad distribution in  $r_{\text{end-end}}$  indicates numerous gauche defects in the majority of the chains. For  $\text{C}_8$  chains at a surface concentration of about  $5.1 \mu\text{mol}/\text{m}^2$  in an environment of pure water and in water-rich aqueous methanol and aqueous acetonitrile, the overall picture is one in which the chains are largely disordered with some lying flat against the surface, while the majority are oriented with  $\chi$  greater than about  $60^\circ$ . The presence of 30 mol % methanol or acetonitrile changes this picture only slightly (compared to the pure water system), with some evidence for a small increase in chain extension.

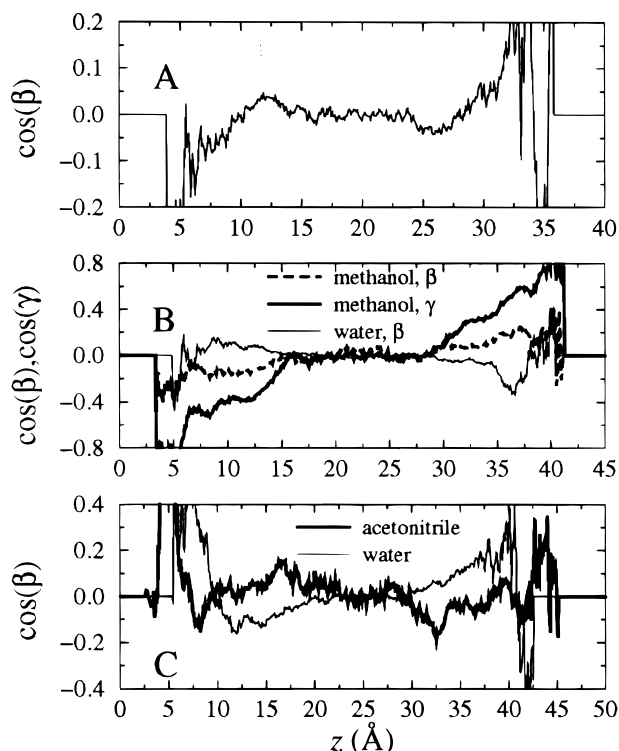


**Figure 9.** Average dipole-wall and bond vector-wall angles as a function of distance in the  $z$  direction, for the (A) pure water, (B) methanol/water, and (C) acetonitrile/water systems.

**4.3. Solvent Orientation.** The average orientation of the solvent as a function of distance in the  $z$  direction has been examined by defining

$$\cos \beta \equiv \hat{d} \cdot \hat{z} \quad \cos \gamma \equiv \hat{b} \cdot \hat{z} \quad (11)$$

where  $\hat{d}$  is the unit dipole vector and  $\hat{b}$  is a unit bond vector pointing from the oxygen to the methyl group on a methanol molecule.  $\hat{z}$  is a unit normal to the wall pointing in the positive direction so that the functions  $\cos \beta(z)$  and  $\cos \gamma(z)$  are expected to be rotationally antisymmetric about  $z_G$ . These results are plotted in Figure 9. In the center, the averages of both  $\cos \beta$  and  $\cos \gamma$  are zero, indicating no preferential orientation of the molecules with respect to the walls. The data become noisier near the ends where the statistics become worse. For the pure water system, the orientation of the water dipole moments near the surface of the hydrocarbon phase is nearly identical with the results for the free interface of pure water.<sup>60</sup> In this case, the sign of  $\cos \beta$  changes at the location of the Gibbs dividing surface, where there is a slight tendency for orientations of the dipole moment toward the bulk for  $z > z_G$  while the reverse is true for  $z < z_G$ . For the mixed-solvent systems, the water dipole moment points more toward the bulk, on average, on both sides of the Gibbs dividing surface in the methanol/water system. This behavior is similar to that seen for free surfaces of water in the presence of submonolayer coverages of phenol.<sup>60</sup> The water in the acetonitrile/water system shows qualitatively different behavior, with the orientation of the water dipole moments being always toward the walls, with the possible exception of the most deeply penetrating water.

The onset of orientational preference of the methanol begins when the number density starts to increase near the interface. These results show that the alignment of the methyl-oxygen bond with the  $z$  axis becomes more and more pronounced as the methanol penetrates deeper into the alkyl chains. Compared

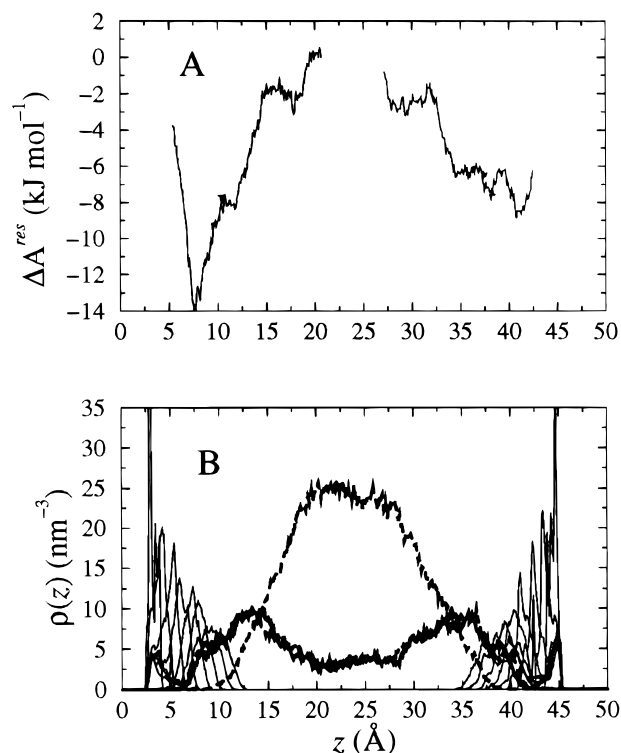


**Figure 10.** (A) Change in residual Helmholtz free energy of a methane solute with position along the  $z$  coordinate. (B) Full density profiles for the acetonitrile/water system. (See legend to Figure 4).

to the methanol, the acetonitrile appears to exhibit less orientational ordering. The interfacial acetonitriles nearest the chains show a small tendency to orient their methyl groups toward the alkyl chains. In contrast, the interfacial acetonitriles nearest the bulk solvent show a tendency to orient their methyl groups toward the bulk fluid, perhaps a manifestation of the antiparallel ordering of the acetonitrile.

**4.4. Free Energy Profile.** The residual Helmholtz free energy profile of a methane solute ( $\sigma = 0.373$  nm,  $\epsilon/k_B = 147.5$  K) in the acetonitrile/water system has been estimated using eq 7 by performing a series of simulations with the starting configuration taken from the ending configuration of the acetonitrile/water simulation discussed above. Two solutes were utilized in each simulation: one was constrained via eq 6 at a position  $z_0$ , while the other was constrained to be at  $L - z_0$ . A total of 11 simulations of lengths  $>90$  ps were run, with the results from each  $z$  window being shifted so that the end points of a window matched the end points of the neighboring windows. These results are displayed in Figure 10 for the solute at  $z_0$  (solid line) and at  $L - z_0$  (dotted line), along with the full density profile for comparison. The qualitative behavior of both solutes is similar, although they do not follow exactly the same path (particularly when the solute resides in the hydrocarbon phase), and there is considerable noise in the results. The differences for the two solutes are an indication of the variability of the local environment found even in a small system. We can, however, note several features of these free energy profile estimates. In particular, there appears to be a small free energy barrier at about  $z = 17$  Å, corresponding to the position of the outer edge of the acetonitrile-rich layer at the hydrocarbon surface, a finding similar to that seen by Klatte and Beck in the methanol/water system at the same bulk mole fraction of organic cosolvent.<sup>30</sup> Once the solute enters the acetonitrile-rich layer at the interface, the free energy drops continuously. At the location



of the second acetonitrile peak at about 8 Å from the wall, the results for the two different solutes are ambiguous, as the free energy continues to drop for one while leveling off for the other solute. In any case, a substantial portion of the total free energy driving force for a methane solute in the acetonitrile system occurs in the organic-rich layer adsorbed to the hydrocarbon phase, a result quite similar to that found previously for a methanol/water/C<sub>18</sub> system.<sup>30</sup> On the basis of the present results, we are therefore unable to identify any distinctly different behavior of a simple spherical solute in the acetonitrile/water system as compared to the methanol/water system, at least at the current composition conditions. We are currently planning investigations of free energy profiles for molecular solutes, such as benzene, with concurrent estimates of the solute energy and entropy profiles as well.

## 5. Concluding Remarks

In this report we have outlined a molecular dynamics model for the study of interphases in reversed-phase liquid chromatography using molecular dynamics simulation. The approach adopted here is one in which the model system is somewhat idealized but, we believe, still captures the essential features of the real system. Further, we have treated the long-ranged electrostatic interactions rigorously with an Ewald sum and derived expressions for the Coulombic contribution to the pressure tensor.

Some features of the model system remain arbitrary, such as the parameters and form of the wall potential and the chain linkage to the wall. However, these simplifications are likely to have little impact on the calculation of the solute free energy profiles, which give a detailed picture of the driving forces behind the retention process.

## 6. Appendix

The Coulombic energy is given by a sum of real-space, reciprocal-space, constant, self, and multipole energies,  $U^C = U_R + U_F + U_{\text{cons}} + U_{\text{self}} + U_m$  where

$$U_R = \sum_i \sum_{j>i} \sum_{\alpha} \sum_{\beta} \sum_{\nu} q_{i\alpha} q_{j\beta} \left\{ \frac{1}{r_{i\alpha j\beta, \nu}} - F_1(\alpha; s_{i\alpha j\beta, \nu}) \right\} \quad (12)$$

$$U_F = \frac{\pi}{A} \sum_{G \neq 0} A_G |G_{\Sigma}|^2 \quad (13)$$

$$U_{\text{cons}} = \frac{1}{2} \sum_i \sum_{\alpha} q_{i\alpha}^2 \sum_{\nu \neq 0} \left\{ \frac{1}{\nu} - F_1(\alpha; \nu) \right\} \quad (14)$$

$$U_{\text{self}} = -\frac{1}{2} \sum_i \sum_{\alpha} q_{i\alpha}^2 \int_0^{\infty} e^{-(\alpha G)^3} dG - \sum_i \sum_{\alpha} \sum_{\beta > \alpha} q_{i\alpha} q_{i\beta} F_1(\alpha; s_{i\alpha i\beta}) \quad (15)$$

$$U_m = \sum_i \sum_{j>i} \sum_{\alpha} \sum_{\beta} q_{i\alpha} q_{j\beta} \times \left\{ -\frac{1}{2} \left( \sum_{\nu} \frac{1}{\nu^3} \right) z_{i\alpha j\beta}^2 + \frac{3}{8} \left( \sum_{\nu} \frac{1}{\nu^5} \right) z_{i\alpha j\beta}^4 - \frac{9}{8} \left( \sum_{\nu} \frac{1}{\nu^5} \right) z_{i\alpha j\beta}^2 s_{i\alpha j\beta}^2 \right\} \quad (16)$$

with

$$F_1(\alpha; \xi) = \int_0^{\infty} J_0(G\xi) e^{-(\alpha G)^3} dG \quad (17)$$

$$A_G = \frac{e^{-(\alpha G)^3}}{G} \quad (18)$$

$$|G_{\Sigma}|^2 = \left[ \left( \sum_i \sum_{\alpha} q_{i\alpha} \cos(\mathbf{G} \cdot \mathbf{s}_{i\alpha}) \right)^2 + \left( \sum_i \sum_{\alpha} q_{i\alpha} \sin(\mathbf{G} \cdot \mathbf{s}_{i\alpha}) \right)^2 \right] \quad (19)$$

$$\sum_{\nu^n} \frac{1}{\nu^n} = \sum_{\{\text{all } \nu\}} \frac{1}{\nu^n} - \sum_{\{\nu_x, \nu_y \leq \nu_c\}} \frac{1}{\nu^n} \quad \nu = L\mathbf{n}, \quad \mathbf{n} = (n_x, n_y), \quad n_x, n_y = 1, 2, 3, \dots \quad (20)$$

where  $q_{i\alpha}$  is the dimensionless fractional charge on site  $\alpha$  of molecule  $i$ ,  $L = L_x = L_y$ ,  $A = L^2$ ,  $\nu$  is a lattice vector,  $\nu_c$  is the lattice vector cutoff,  $J_0$  is the zeroth-order Bessel function of the first kind,<sup>61</sup> and  $\mathbf{G}$  are reciprocal lattice vectors in the  $x$ - $y$  plane. Note that in the above equations the factor  $1/4\pi\epsilon_0$  has been omitted.  $s$  and  $z$  are the  $x$ - $y$  and  $z$  components of the positions. The forces are obtained straightforwardly by differentiation:

$$\mathbf{F}_{Ri\alpha j\beta}^s = \sum_i \sum_{j>i} \sum_{\alpha} \sum_{\beta} \sum_{\nu} q_{i\alpha} q_{j\beta} \left\{ \frac{1}{r_{i\alpha j\beta, \nu}^3} - F_2(\alpha; s_{i\alpha j\beta, \nu}) \right\} \mathbf{s}_{i\alpha j\beta, \nu} \quad (21)$$

$$\mathbf{F}_R^z = \sum_i \sum_{j>i} \sum_{\alpha} \sum_{\beta} \sum_{\nu} q_{i\alpha} q_{j\beta} \frac{z_{i\alpha j\beta}}{r_{i\alpha j\beta, \nu}^3} \quad (22)$$

$$\mathbf{F}_m^s = \sum_i \sum_{j>i} \sum_{\alpha} \sum_{\beta} q_{i\alpha} q_{j\beta} \frac{9}{4} \left( \sum_{\nu} \frac{1}{\nu^5} \right) z_{i\alpha j\beta}^2 \mathbf{s}_{i\alpha j\beta} \quad (23)$$

$$\mathbf{F}_m^z = \sum_i \sum_{j>i} \sum_{\alpha} \sum_{\beta} q_{i\alpha} q_{j\beta} \left\{ \sum_{\nu} \frac{1}{\nu^3} - \frac{3}{2} \left( \sum_{\nu} \frac{1}{\nu^5} \right) z_{i\alpha j\beta}^2 + \frac{9}{4} \left( \sum_{\nu} \frac{1}{\nu^5} \right) s_{i\alpha j\beta}^2 \right\} \mathbf{z}_{i\alpha j\beta} \quad (24)$$

$$\mathbf{F}_F = \frac{2\pi}{A} \sum_{G \neq 0} A_G \mathbf{G} \left[ \left( \sum_i \sum_{\alpha} \cos(\mathbf{G} \cdot \mathbf{s}_{i\alpha}) q_{i\alpha} \sin(\mathbf{G} \cdot \mathbf{s}_{i\alpha}) - \left( \sum_i \sum_{\alpha} \sin(\mathbf{G} \cdot \mathbf{s}_{i\alpha}) q_{i\alpha} \cos(\mathbf{G} \cdot \mathbf{s}_{i\alpha}) \right) \right] \quad (25)$$

where

$$F_2(\alpha; \xi) = \frac{1}{\xi} \int_0^{\infty} J_1(G\xi) G e^{-(\alpha G)^3} dG$$

and  $J_1$  is the first-order Bessel function of the first kind.<sup>61</sup> In practice, the Bessel functions  $J_0$  and  $J_1$  are computed using polynomial representations found in ref 62. After choosing an appropriate value for the convergence parameter  $\alpha$ , the functions  $F_1$  and  $F_2$  are tabulated and their values interpolated linearly during the program execution.

In the molecular formulation, the Coulombic contribution to the pressure tensor is given by  $\mathbf{P}^C = \mathbf{P}^R + \mathbf{P}^F + \mathbf{P}^m + \mathbf{P}^{\text{cons}}$ , where, following the development in the 3DP Ewald formulation of Nosé and Klein<sup>63</sup> and Brown and Neyertz,<sup>64</sup> we have, for the  $(\alpha, \beta)$  component



$$VP_{\alpha\beta}^R = \sum_i \sum_{j>i} \sum_{\gamma} \sum_{\mu} \sum_{\nu} (R_{ij,\nu})_{\alpha} (F_{ij\mu,\nu}^R)_{\beta} \quad (26)$$

$$VP_{\alpha\beta}^F = \frac{\pi}{A} \sum_{G \neq 0} A_G \left( \delta_{\alpha\beta} - \left( 3\alpha^3 G + \frac{1}{G^2} \right) G_{\alpha} G_{\beta} \right) |G_{\Sigma}|^2 + \frac{2\pi}{A} \sum_{G \neq 0} \times \\ \{ A_G [ (\sum_i \sum_{\gamma} q_{i\gamma} \sin(\mathbf{G} \cdot \mathbf{s}_{i\gamma})) (\sum_i \sum_{\gamma} q_{i\gamma} \cos(\mathbf{G} \cdot \mathbf{s}_{i\gamma}) G_{\alpha} (d_{i\gamma})_{\beta}) - \\ (\sum_i \sum_{\gamma} q_{i\gamma} \cos(\mathbf{G} \cdot \mathbf{s}_{i\gamma})) (\sum_i \sum_{\gamma} q_{i\gamma} \sin(\mathbf{G} \cdot \mathbf{s}_{i\gamma}) G_{\alpha} (d_{i\gamma})_{\beta}) ] \} \quad (27)$$

$$VP_{\alpha\beta}^{cons} = \frac{1}{2} \sum_i \sum_{\gamma} q_{i\gamma}^2 \sum_{\nu \neq 0} \left\{ \frac{\nu_{\alpha} \nu_{\beta}}{\nu^3} - \nu_{\alpha} \nu_{\beta} F_2(\alpha; \nu) \right\} \quad (28)$$

$$VP_{\alpha\beta}^m = \sum_i \sum_{j>i} \sum_{\gamma} \sum_{\mu} (R_{ij,\nu})_{\alpha} (F_{ij\mu,\nu}^m)_{\beta} + \\ \sum_i \sum_{j>i} \sum_{\gamma} \sum_{\mu} q_{i\gamma} q_{j\mu} \left\{ \frac{-3}{2} \left( \sum'_{\nu} \frac{\nu_{\alpha} \nu_{\beta}}{\nu^5} \right) z_{ij\mu}^2 + \right. \\ \left. \frac{15}{8} \left( \sum'_{\nu} \frac{\nu_{\alpha} \nu_{\beta}}{\nu^7} \right) z_{ij\mu}^4 - \frac{45}{8} \left( \sum'_{\nu} \frac{\nu_{\alpha} \nu_{\beta}}{\nu^7} \right) z_{ij\mu}^2 s_{ij\mu}^2 \right\} \quad (29)$$

where  $\delta_{\alpha\beta}$  is the Kronecker delta.

The atomic formulation of the pressure tensor includes the intramolecular forces, and its Coulombic contribution is the same as the molecular pressure tensor, with  $(R_{ij,\nu})_{\alpha}$  and  $(R_{ij})_{\alpha}$  replaced by  $(r_{ij\mu,\nu})_{\alpha}$  and  $(r_{ij\mu})_{\alpha}$ , and dropping the second term in  $P_{\alpha\beta}^F$ . Furthermore, by symmetry, the off-diagonal terms in  $P_{\alpha\beta}^{cons}$  and in the second term of  $P_{\alpha\beta}^m$  are zero.

For spherical ions, we also have the well-known result that, which provides a convenient check for the above expressions. A test calculation of 256 KCl ions yielded agreement in the last expression to within numerical error.

The total pressure tensor in the "atomic" framework is given by

$$\mathbf{P} = \mathbf{P}^C + \mathbf{P}^{LJ} + \mathbf{P}^{tors} + \mathbf{P}^{bend} + \mathbf{P}^{LJ,intra} + \mathbf{P}^{constraint} + \mathbf{P}^{wall} + \mathbf{P}^{spring} \quad (30)$$

where  $\mathbf{P}^{LJ}$  is the intermolecular contribution due to Lennard-Jones interactions,  $\mathbf{P}^{tors}$ ,  $\mathbf{P}^{bend}$ , and  $\mathbf{P}^{LJ,intra}$  are contributions from the intramolecular potential of the chains,  $\mathbf{P}^{constraint}$  is the constraint force contribution, and  $\mathbf{P}^{wall}$  and  $\mathbf{P}^{spring}$  are contributions from the wall and the spring attached to the first site of the  $C_8$  chains.

## References and Notes

- Dorsey, J. G.; Dill, K. A. *Chem. Rev.* **1989**, 89, 331.
- Carr, P. W.; Li, J.; Dallas, A. J.; Eikens, D. I.; Tan, L. C. *J. Chromatogr. A* **1993**, 656, 113.
- Berendsen, G. E.; Galan, L. D. *J. Chromat.* **1980**, 196, 21.
- Kohler, J.; Chase, D. B.; Faile, R. D.; Vega, A. J.; Kirkland, J. J. *J. Chromatogr.* **1986**, 352, 275.
- Roumeliotis, P.; Unger, K. K. *J. Chromatogr.* **1978**, 149, 211.
- Kirkland, J. J.; Glajch, J. L.; Farbe, R. D. *Anal. Chem.* **1989**, 61, 2.
- Lochmüller, C. H.; Colborn, A. S.; Hunnicutt, M. L.; Harris, J. M. *Anal. Chem.* **1983**, 55, 1344.
- Marqusee, J. A.; Dill, K. A. *J. Chem. Phys.* **1986**, 85, 434.
- Horváth, C.; Melander, W.; Molnár, I. *J. Chromatogr.* **1976**, 125, 129.
- Dill, K. A. *J. Phys. Chem.* **1987**, 91, 1980.
- Sentell, K. B.; Dorsey, J. G. *J. Chromatogr.* **1989**, 461, 193.
- Alvarez-Zepeda, A.; Barman, B. N.; Martire, D. E. *Anal. Chem.* **1992**, 64, 1978.
- Bliesner, D. M.; Sentell, K. B. *Anal. Chem.* **1993**, 65, 1819.
- M. E. Montgomery, J.; Green, M. A.; Wirth, M. J. *Anal. Chem.* **1992**, 64, 1170.
- Wise, S. A.; Bonnett, W. J.; Guenther, F. R.; May, W. E. *J. Chromatogr. Sci.* **1981**, 19, 457.
- Wise, S. A.; Sander, L. C. *J. High Resolut. Chromatogr. Chromatogr. Commun.* **1985**, 8, 248.
- Guillaume, Y. C.; Gunichard, C. *Anal. Chem.* **1996**, 68, 2869.
- Stalcup, A. M.; Martire, D. E.; Wise, S. A. *J. Chromatogr. A* **1988**, 442, 1.
- Balakrishnan, S.; Eastale, A. J. *Aust. J. Chem.* **1981**, 34, 943.
- Carr, P. W.; Doherty, R. M.; Kamlet, M. J.; Taft, R. W.; Melander, W.; Horvath, C. *Anal. Chem.* **1986**, 58, 2674.
- Johnson, B. P.; Khaleli, M. G.; Dorsey, J. G. *Anal. Chem.* **1986**, 58, 2354.
- Hanai, T.; Jukurogi, A.; Hubert, J. *Chromatographia* **1984**, 19, 266.
- Rowlen, K. L.; Harris, J. M. *Anal. Chem.* **1991**, 63, 964.
- Marcus, Y.; Migron, Y. *J. Phys. Chem.* **1991**, 95, 400.
- Gray, C. G.; Gubbins, K. E.; *Theory of Molecular Fluids*; Clarendon Press: Oxford, U.K., 1984; Vol. I.
- Sander, L. C.; Callis, J. B.; Field, L. R. *Anal. Chem.* **1983**, 55, 1068.
- Cole, L. A.; Dorsey, J. G. *Anal. Chem.* **1992**, 64, 1317.
- Cole, L. A.; Dorsey, J. G.; Dill, K. A. *Anal. Chem.* **1992**, 64, 1324.
- Katz, E. D.; Ogan, K.; Scott, R. P. W. *J. Chromatogr.* **1986**, 352, 67.
- Klatte, S. J.; Beck, T. L. *J. Phys. Chem.* **1996**, 100, 5931.
- Snook, I. K.; van Megen, W.; *J. Chem. Phys.* **1980**, 72, 2907.
- Ryckaert, J.-P.; Bellemans, A. *Discuss. Faraday Soc.* **1978**, 66, 95.
- Böcker, J.; Schlenkrich, M.; Bopp, P.; Brickmann, J. *J. Phys. Chem.* **1992**, 96, 9915.
- Bekker, H.; Berendsen, H. J. C.; van Gunsteren, W. F. *J. Comput. Chem.* **1995**, 16, 527.
- Berendsen, H. J. C.; Postma, J. P. M.; van Gunsteren, W. F.; Hermans, J. In *Intermolecular Forces*; Pullman, B., Ed.; D. Reidel: Dordrecht, The Netherlands, 1981; pp 331–342.
- van Leeuwen, M. E. Molecular simulation of the phase behaviour of polar fluids. Ph.D. Thesis, Universiteit Utrecht, The Netherlands.
- Edwards, D. M. F.; Madden, P. A.; McDonald, I. R. *Mol. Phys.* **1984**, 51, 1141.
- Slusher, J. T.; Cummings, P. T. *Mol. Sim.* **1996**, 18, 213.
- Beeman, D. *J. Comput. Phys.* **1976**, 20, 130.
- Melchionna, S.; Ciccotti, G.; Holian, B. L. *Mol. Phys.* **1993**, 78, 533.
- Rhee, Y.-H.; Halley, J. W.; Hautman, J.; Rahman, A. *Phys. Rev. B* **1989**, 40, 36.
- Smith, E. R. *Mol. Phys.* **1988**, 65, 1089.
- Alejandro, J.; Tildesley, D. J.; Chapela, G. A. *J. Chem. Phys.* **1995**, 102, 4574.
- Feller, S. E.; Pastor, R. W.; Rojnuckarin, A.; Bogusz, S.; Brooks, B. R. *J. Phys. Chem.* **1996**, 100, 17011.
- Widmann, A. H.; Adolf, D. B. *Comput. Phys. Comm.* **1997**, 107, 167.
- Hautman, J.; Klein, M. L. *Mol. Phys.* **1992**, 75, 379.
- Leckner, J. *Physica A* **1991**, 176, 485.
- Heyes, D. M.; Barber, M.; Clarke, J. H. R.; *J. Chem. Soc., Faraday Trans. 2* **1977**, 73, 1485.
- Sander, L. C.; Wise, S. A. In *Retention and Selectivity in Liquid Chromatography*; Smith, R. M., Ed.; Elsevier Science: Amsterdam, 1995; Vol. 57, p 337.
- Chandler, D. *Introduction to modern statistical mechanics*; Oxford University Press: New York, 1987; pp 168–175.
- Jönsson, B. *Chem. Phys. Lett.* **1981**, 82, 520.
- Marchesi, M. *Chem. Phys. Lett.* **1983**, 97, 224.
- Lee, C. Y.; McCammon, J. A. *J. Chem. Phys.* **1984**, 80, 4448.
- Christou, N. I.; Whitehouse, J. S.; Nicholson, D.; Parsonage, N. G. *Mol. Phys.* **1985**, 55, 397.
- Michael, D.; Benjamin, I. *J. Phys. Chem.* **1995**, 99, 1530.
- Benjamin, I. *J. Chem. Phys.* **1992**, 97, 1432.
- Pohorille, A.; Wilson, M. A. *J. Mol. Struct. (THEOCHEM)* **1993**, 284, 271.
- Gilpin, R. K.; Squires, J. A. *J. Chromatogr. Sci.* **1981**, 19, 195.
- Gilpin, R. K.; Gangoda, M. E.; Krishen, A. E. *J. Chromatograph. Sci.* **1982**, 20, 345.
- Sokhan, V. P.; Tildesley, D. J. *Mol. Phys.* **1997**, 92, 625.
- Hildebrand, F. B. *Advanced Calculus for Applications*, 2nd ed.; Prentice-Hall: Englewood Cliffs, NJ, 1976.
- Abramowitz, M.; Stegun, I. R., Eds. *Handbook of mathematical functions*; U.S. Department of Commerce, Washington, DC, 1964.
- Nosé, S.; Klein, M. L. *Mol. Phys.* **1983**, 50, 1055.
- Brown, D.; Neyertz, S. *Mol. Phys.* **1995**, 84, 577.